Experimental verification of epsilon-near-zero plasmon polariton modes in degenerately doped semiconductor nanolayers

Salvatore Campione,[1,2,*] Iltai Kim,[1,2,3] Domenico de Ceglia,[4] Gordon A. Keeler,[2] and Ting S. Luk[1,2,5]

[1]*Center for Integrated Nanotechnologies (CINT), Sandia National Laboratories, P.O. Box 5800, Albuquerque, NM 87185, USA*
[2]*Sandia National Laboratories, P.O. Box 5800, Albuquerque, NM 87185, USA*
[3]*Currently with the School of Engineering & Computing Science, Texas A&M University-Corpus Christi, Corpus Christi, Texas 78412, USA*
[4]*National Research Council – AMRDEC, Charles M. Bowden Research Laboratory, Redstone Arsenal, AL, 35898 USA*
[5]*tsluk@sandia.gov*
[*]*sncampi@sandia.gov*

Abstract: We investigate optical polariton modes supported by subwavelength-thick degenerately doped semiconductor nanolayers (e.g. indium tin oxide) on glass in the epsilon-near-zero (ENZ) regime. The dispersions of the radiative (R, on the left of the light line) and non-radiative (NR, on the right of the light line) ENZ polariton modes are experimentally measured and theoretically analyzed through the transfer matrix method and the complex-frequency/real-wavenumber analysis, which are in remarkable agreement. We observe directional near-perfect absorption using the Kretschmann geometry for incidence conditions close to the NR-ENZ polariton mode dispersion. Along with field enhancement, this provides us with an unexplored pathway to enhance nonlinear optical processes and to open up directions for ultrafast, tunable thermal emission.

OCIS codes: (240.0310) Thin films; (310.6628) Subwavelength structures, nanostructures; (310.6860) Thin films, optical properties; (240.6680) Surface plasmons.

References and Links

1. K. L. Kliewer and R. Fuchs, "Optical modes of vibration in an ionic crystal slab including retardation. I. Nonradiative region," Phys. Rev. **144**(2), 495–503 (1966).
2. K. L. Kliewer and R. Fuchs, "Optical modes of vibration in an ionic crystal slab including retardation. II. Radiative region," Phys. Rev. **150**(2), 573–588 (1966).
3. R. Fuchs, K. L. Kliewer, and W. J. Pardee, "Optical properties of an ionic crystal slab," Phys. Rev. **150**(2), 589–596 (1966).
4. R. Ruppin and R. Englman, "Optical phonons of small crystals," Rep. Prog. Phys. **33**(1), 149–196 (1970).
5. M. Schubert, *Infrared Ellipsometry on Semiconductor Layer Structures* (Springer, 2004).
6. D. Sarid, "Long-range surface-plasma waves on very thin metal films," Phys. Rev. Lett. **47**(26), 1927–1930 (1981).
7. E. N. Economou, "Surface plasmons in thin films," Phys. Rev. **182**(2), 539–554 (1969).
8. J. M. Pitarke, V. M. Silkin, E. V. Chulkov, and P. M. Echenique, "Surface plasmons in metallic structures," J. Opt. A, Pure Appl. Opt. **7**(2), S73–S84 (2005).
9. R. P. Godwin and M. M. Mueller, "Reflection spectroscopy by plasma-resonance enhancement," Appl. Opt. **12**(6), 1276–1278 (1973).
10. B. Harbecke, B. Heinz, and P. Grosse, "Optical properties of thin films and the Berreman effect," Appl. Phys., A Mater. Sci. Process. **38**(4), 263–267 (1985).
11. D. W. Berreman, "Infrared absorption at longitudinal optic frequency in cubic crystal films," Phys. Rev. **130**(6), 2193–2198 (1963).
12. T. S. Luk, S. Campione, I. Kim, S. Feng, Y. C. Jun, S. Liu, J. B. Wright, I. Brener, P. B. Catrysse, S. Fan, and M. B. Sinclair, "Directional perfect absorption using deep subwavelength low-permittivity films," Phys. Rev. B **90**(8), 085411 (2014).
13. J. J. Burke, G. I. Stegeman, and T. Tamir, "Surface-polariton-like waves guided by thin, lossy metal films," Phys. Rev. B Condens. Matter **33**(8), 5186–5201 (1986).

14. M. A. Badsha, Y. C. Jun, and C. K. Hwangbo, "Admittance matching analysis of perfect absorption in unpatterned thin films," Opt. Commun. **332**, 206–213 (2014).
15. S. Vassant, J. P. Hugonin, F. Marquier, and J. J. Greffet, "Berreman mode and epsilon near zero mode," Opt. Express **20**(21), 23971–23977 (2012).
16. T. Taliercio, V. N. Guilengui, L. Cerutti, E. Tournié, and J.-J. Greffet, "Brewster "mode" in highly doped semiconductor layers: an all-optical technique to monitor doping concentration," Opt. Express **22**(20), 24294–24303 (2014).
17. J. Bösenberg and H. Raether, "Plasma-resonance emission of potassium, excited by light," Phys. Rev. Lett. **18**(11), 397–398 (1967).
18. E. A. Vinogradov, G. N. Zhizhin, A. G. Mal'shukov, and V. I. Yudson, "Thermostimulated polariton emission of zinc selenide films on metal substrate," Solid State Commun. **23**(12), 915–921 (1977).
19. R. A. Ferrell, "Predicted radiation of plasma oscillations in metal films," Phys. Rev. **111**(5), 1214–1222 (1958).
20. A. Bichri, J. Lafait, and H. Welsch, "Visible and infrared optical properties of Ag/SiO_2 multilayers: radiative virtual modes and coupling effects," J. Phys. Condens. Matter **5**(40), 7361–7374 (1993).
21. A. J. McAlister and E. A. Stern, "Plasma resonance absorption in thin metal films," Phys. Rev. **132**(4), 1599–1602 (1963).
22. S. Vassant, A. Archambault, F. Marquier, F. Pardo, U. Gennser, A. Cavanna, J. L. Pelouard, and J. J. Greffet, "Epsilon-near-zero mode for active optoelectronic devices," Phys. Rev. Lett. **109**(23), 237401 (2012).
23. S. Campione, I. Brener, and F. Marquier, "Theory of epsilon-near-zero modes in ultrathin films," Phys. Rev. B **91**(12), 121408 (2015).
24. M. Z. Alam, I. De Leon, and R. W. Boyd, "Large optical nonlinearity of indium tin oxide in its epsilon-near-zero region," Science **352**(6287), 795–797 (2016).
25. L. Caspani, R. P. M. Kaipurath, M. Clerici, M. Ferrera, T. Roger, J. Kim, N. Kinsey, M. Pietrzyk, A. Di Falco, V. M. Shalaev, A. Boltasseva, and D. Faccio, "Enhanced nonlinear refractive index in ε-near-zero materials," Phys. Rev. Lett. **116**(23), 233901 (2016).
26. S. Franzen, C. Rhodes, M. Cerruti, R. W. Gerber, M. Losego, J.-P. Maria, and D. E. Aspnes, "Plasmonic phenomena in indium tin oxide and ITO-Au hybrid films," Opt. Lett. **34**(18), 2867–2869 (2009).
27. L. Dominici, F. Michelotti, T. M. Brown, A. Reale, and A. Di Carlo, "Plasmon polaritons in the near infrared on fluorine doped tin oxide films," Opt. Express **17**(12), 10155–10167 (2009).
28. Y. C. Jun, J. Reno, T. Ribaudo, E. Shaner, J.-J. Greffet, S. Vassant, F. Marquier, M. Sinclair, and I. Brener, "Epsilon-near-zero strong coupling in metamaterial-semiconductor hybrid structures," Nano Lett. **13**(11), 5391–5396 (2013).
29. S. Campione, D. de Ceglia, M. A. Vincenti, M. Scalora, and F. Capolino, "Electric field enhancement in ε-near-zero slabs under TM-polarized oblique incidence," Phys. Rev. B **87**(3), 035120 (2013).
30. D. de Ceglia, S. Campione, M. A. Vincenti, F. Capolino, and M. Scalora, "Low-damping epsilon-near-zero slabs: Nonlinear and nonlocal optical properties," Phys. Rev. B **87**(15), 155140 (2013).
31. A. Alù, M. G. Silveirinha, A. Salandrino, and N. Engheta, "Epsilon-near-zero metamaterials and electromagnetic sources: Tailoring the radiation phase pattern," Phys. Rev. B **75**(15), 155410 (2007).
32. M. Antonietta Vincenti, S. Campione, D. de Ceglia, F. Capolino, and M. Scalora, "Gain-assisted harmonic generation in near-zero permittivity metamaterials made of plasmonic nanoshells," New J. Phys. **14**(10), 103016 (2012).
33. M. A. Vincenti, D. de Ceglia, A. Ciattoni, and M. Scalora, "Singularity-driven second- and third-harmonic generation at ε -near-zero crossing points," Phys. Rev. A **84**(6), 063826 (2011).
34. C. Argyropoulos, P.-Y. Chen, G. D'Aguanno, N. Engheta, and A. Alù, "Boosting optical nonlinearities in ε -near-zero plasmonic channels," Phys. Rev. B **85**(4), 045129 (2012).
35. C. Argyropoulos, G. D'Aguanno, and A. Alù, "Giant second-harmonic generation efficiency and ideal phase matching with a double ε-near-zero cross-slit metamaterial," Phys. Rev. B **89**(23), 235401 (2014).
36. M. A. Vincenti, D. de Ceglia, J. W. Haus, and M. Scalora, "Harmonic generation in multiresonant plasma films," Phys. Rev. A **88**(4), 043812 (2013).
37. T. S. Luk, D. de Ceglia, S. Liu, G. A. Keeler, R. P. Prasankumar, M. A. Vincenti, M. Scalora, M. B. Sinclair, and S. Campione, "Enhanced third harmonic generation from the epsilon-near-zero modes of ultrathin films," Appl. Phys. Lett. **106**(15), 151103 (2015).
38. A. Capretti, Y. Wang, N. Engheta, and L. Dal Negro, "Enhanced third-harmonic generation in Si-compatible epsilon-near-zero indium tin oxide nanolayers," Opt. Lett. **40**(7), 1500–1503 (2015).
39. T. S. Luk, I. Kim, S. Campione, S. W. Howell, G. S. Subramania, R. K. Grubbs, I. Brener, H.-T. Chen, S. Fan, and M. B. Sinclair, "Near-infrared surface plasmon polariton dispersion control with hyperbolic metamaterials," Opt. Express **21**(9), 11107–11114 (2013).
40. M. Born and E. Wolf, *Principles of Optics: Electromagnetic Theory of Propagation, Interference, and Diffraction of Light* (Cambridge University, 1999).
41. D. M. Pozar, *Microwave Engineering* (John Wiley and Sons, 2011).

1. Introduction

Optical polaritons of light and optical phonon interactions were explored extensively in the past [1–8]. The theoretical results of Godwin and Mueller [9] pointed to the possibility that a

strong absorption of *p*-polarized light could be achieved near the plasma frequency of a layer of diluted plasma backed by a metal. Similarly, Harbecke et al. [10] theoretically showed strong absorption near the SiO_2 longitudinal optical phonon frequency in metal backed films. The appearance of this absorption peak is known as the Berreman effect [10, 11]. In a similar fashion, absorption peaks can be also observed for plasmonic materials [12–14]. The Berreman effect was recently attributed to the excitation of a radiative mode supported by the layered environment [15, 16]. Prior to such definition, however, many studies have confirmed the existence of the Berreman effect [17–21]. Such effect was associated to a collective plasma oscillation in thin films in correspondence of an epsilon-near-zero (ENZ) crossing point. This mode resides on the radiative side (left side) of the light line [15]. For this reason, we refer to it as the radiative ENZ (R-ENZ) plasmon polariton mode. The non-radiative counter part of this mode was referred to as ENZ mode in [15], and its dispersion has yet to be proven experimentally. This mode corresponds to a long-range surface plasmon polariton mode in the thin-film regime [22, 23]. To express its physical origin, here we refer to it as the non-radiative ENZ (NR-ENZ) plasmon polariton mode. While the dispersion properties of these modes have been discussed theoretically [15, 22, 23] and very recently experimentally only for the R-ENZ branch [16], detailed experimental measurements of the NR-ENZ mode has not been yet shown. The latter verification is important, for example, for usage of this mode for ultrafast, tunable thermal emission or ultrafast nonlinear optical response [24, 25], and is the main goal of this paper.

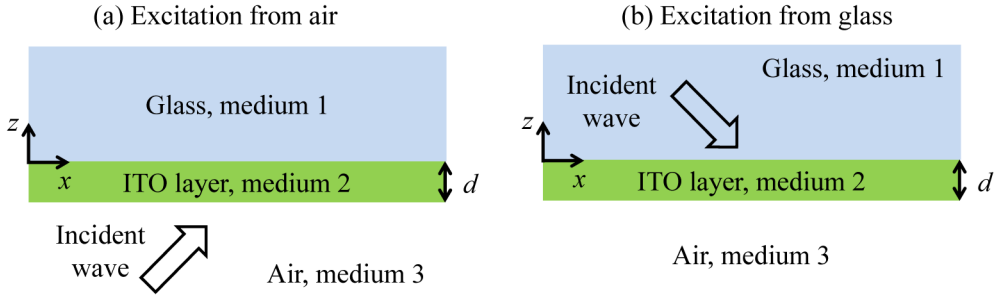

Fig. 1. Schematic depiction of a three-medium structure comprising a half space made of glass (medium 1), a subwavelength ITO layer of thickness *d* (medium 2), and a half space made of air (medium 3) with oblique, *p*-polarized plane wave excitation from (a) air and (b) glass using the Kretschmann geometry. The excitation schemes in (a) and (b) are used to trace the dispersions of the R-ENZ and the NR-ENZ polariton modes, respectively.

Here, we report the experimental dispersions of both R-ENZ and NR-ENZ plasmon polariton modes supported by an unpatterned deep sub-wavelength indium tin oxide (ITO) film on top of a glass substrate without metal as back reflector, as shown in Fig. 1. Note that, although the structure in [15] is different from the one employed in this work (metal substrate in [15] and glass in the present work), many of the important properties of the ENZ modes are similar for the two configurations. In Sec. 2, we show that the R-ENZ plasmon polariton mode is measured by exciting from the air side [Fig. 1(a)], while the NR-ENZ plasmon polariton mode is measured by exciting from the glass side using the Kretschmann geometry [Fig. 1(b)]. We find that such dispersions are in very good agreement with transfer matrix method (TMM) calculations. Moreover, we show in Sec. 3 that such dispersions are also in good agreement with the analysis of the electromagnetic eigenmodes of the three-medium structure using complex-frequencies and real-wavenumbers. These computations allow us to find two modes whose dispersions agree significantly well with the experimental ones. These modes are different from the standard surface plasmon polariton (SPP) mode [26, 27] because of the thin-film condition: the electric field magnitude is maximum inside the film for ENZ modes rather than minimum for SPP modes [15, 22, 28]. We then observe in Sec. 4 near-perfect absorption (near-PA) even without a metal substrate for illumination conditions close

to the NR-ENZ polariton mode dispersion. With the proper thickness, PA is possible. This is a remarkable result given the deep sub-wavelength extent of the ITO layer used here (one sample has a thickness of 24 nm, about 1/50th of the free space wavelength of 1.1 μm). This is important in case absorbing materials without metals are required for device applications because beyond the critical angle the structure behaves exactly like a back-mirrored thin film. This near-PA happens close to the ENZ frequency point, and is a result of a significantly enhanced electric field that is strongly confined in films of subwavelength thickness due to the NR-ENZ polariton mode [15, 29–31]. Alternatively, for thin-film configurations that exhibit low reflectivity near the ENZ frequency, the continuity of the normal component of the electric displacement necessarily requires the existence of a large electric field immediately inside the film [29]. However, such low reflectivity can only be achieved through excitation of a thin film resonance, which in the present case is the NR-ENZ mode. This property might be pivotal for the enhancement of nonlinear processes, such as second and third harmonic generation, and multistability phenomena [30, 32–38].

2. Experimental verification of epsilon-near-zero plasmon polariton modes

Our experimental verification of the dispersions of the R-ENZ and NR-ENZ plasmon polariton modes in ultrathin ENZ films utilizes the three-medium structure shown in Fig. 1. It comprises a half space made of glass (medium 1, with relative permittivity ε_1), an ultrathin ITO layer with thickness d (medium 2, with relative permittivity ε_2), and a half space made of air (medium 3, with relative permittivity ε_3). The experimental samples are fabricated as follows. The ITO films were deposited on boroaluminosilicate glass substrates using a 90 wt% In_2O_3 /10 wt% SnO_2 sputtering target at room temperature under a base vacuum pressure of 10^{-7} torr, followed by a 10 minute anneal in Ar gas at 700 °C. Two samples were prepared with differing ITO thicknesses of d = 24 and 53 nm. We do not tune the ITO carrier concentration, which is kept the same for all samples. The small differences we observe in concentration are only due to variations inherent in the process. The permittivity functions of the two films in the spectral range of 0.3–2.5 μm were obtained through spectroscopic ellipsometry measurements, using a combination of Drude and Gaussian models. These are shown in Fig. 2(a) for the two samples.

The frequency dependence of the reflectivity R was measured using a spectroscopic ellipsometer (J.A. Woollam, Inc.) for fixed incidence angles. For the dispersion measurement of the two modes, the optical waves are incident on the ITO film in different manner, depending on the mode of interest. For the dispersion of the NR-ENZ polariton mode on the right of the light line, the incidence is from the glass side using the Kretschmann geometry as depicted in Fig. 1(b) [curves for two angles are reported in the inset of Fig. 2(b)]. For these measurements, the incident beam was coupled to the sample through a BK7 glass prism that was index matched to the glass substrate of the sample, with one of the ITO surfaces exposed to air similar to previous measurements [12, 39]. For the dispersion of the R-ENZ polariton mode on the left of the light line, the incidence is from the air side as depicted in Fig. 1(a). For each incidence angle, we identify the resonance frequency corresponding to a peak in the absorption spectrum, and thus map the experimental dispersions of the two modes in Fig. 2 depicted by blue circles (for the 24 nm sample) and green triangles (for the 53 nm sample). TMM results (blue and green dashed lines for the 24 nm and the 53 nm samples, respectively) were performed in a similar way accounting for the ITO measured permittivity functions in Fig. 2(a). A good agreement is observed between experimental and TMM results for both ITO samples analyzed in this paper.

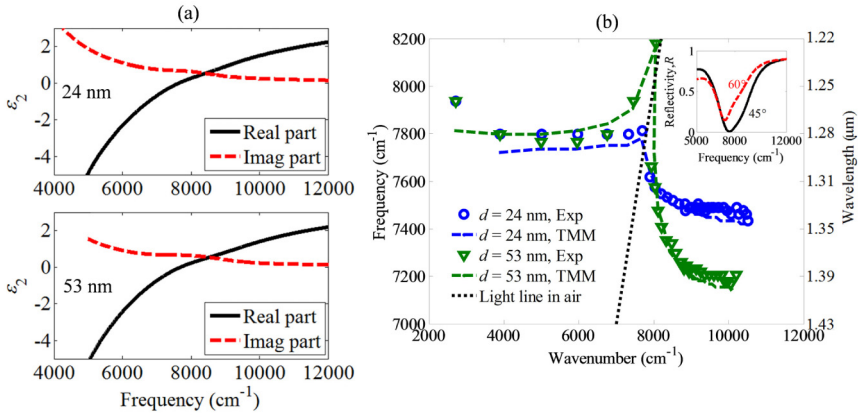

Fig. 2. (a) Real and imaginary parts of the ITO permittivity for the two samples with thicknesses of 24 and 53 nm. The ENZ crossing point is at ~7650 cm^{-1} (24 nm) and ~7700 cm^{-1} (53 nm). (b) Frequency/wavenumber dispersion diagram retrieved both experimentally (Exp) and via transfer matrix method (TMM) simulations for the two samples under analysis with thicknesses of 24 (blue circles and dashed blue line) and 53 (green triangles and green dashed line) nm. The data on the right of the light line was obtained using the excitation scheme in Fig. 1(b); the one on the left of the light line was obtained using the excitation scheme in Fig. 1(a). The inset reports two experimental reflectivity spectra for the 53 nm sample for the incident angles of 45 (black solid) and 60 (red dashed) degrees for the excitation scheme in Fig. 1(b).

3. Complex-frequency/real-wavenumber modal analysis

Because the results in Fig. 2 are obtained via different excitation schemes as required by the R-ENZ and the NR-ENZ polariton modes, we infer that each branch on the left and on the right of the light line will pertain to a different eigenmode supported by the three-medium structure. These eigenmodes will be studied in what follows to get a physical understanding of the two dispersions. Assuming a reference plane at the center of the ITO layer, the complex-frequency/real-wavenumber dispersion diagrams can be obtained by finding the complex roots of

$$Z_t = Z_u + Z_d = 0 \tag{1}$$

for *p*-polarized waves, where

$$Z_u = \frac{A_2 Z_1 + B_2}{C_2 Z_1 + D_2} \text{ and } Z_d = \frac{A_2 Z_3 + B_2}{C_2 Z_3 + D_2} \tag{2}$$

are the wave impedances of medium 1 and of medium 3 transferred to the center of the ITO layer (reference plane), respectively. This is fully equivalent to finding the complex roots of the denominator of the Fresnel reflection coefficient [12, 40]. In Eq. (2), $A_2 = D_2 = \cos(k_{z2} d/2)$, $B_2 = -iZ_2 \sin(k_{z2} d/2)$, and $C_2 = -i\sin(k_{z2} d/2)/Z_2$ are the ABCD parameters of the ITO layer [41] [the monochromatic time harmonic convention $\exp(-i\omega t)$ is implicitly assumed]. Note that for *p*-polarized waves, the wave impedances of each layer become $Z_n = k_{zn}/(\omega\varepsilon_0\varepsilon_n)$, where $k_{zn}^2 = k_n^2 - k_x^2$, $n = 1,2,3$, $k_n^2 = k_0^2\varepsilon_n$, ε_0 is the absolute permittivity of free space and ω is the angular frequency. Then, to find the eigenmodes, we fix the (real) wavenumber k_x in the *x*-direction and find the complex angular frequency by calculating the roots of Eq. (1). We stress that since we are looking for a complex angular frequency solution we use here an approximate, analytical Drude model equation for the ITO permittivity that fits the experimental data from ellipsometry shown in

Fig. 2(a) [$\varepsilon_{\mathrm{ITO}} = \varepsilon_\infty - \dfrac{\omega_p^2}{\omega(\omega + i\gamma)}$ with $\varepsilon_\infty = 3.993$, $\omega_p = 2.89\times10^{15}$ rad/s, and $\gamma = 2.1\times10^{14}$ rad/s for the 24 nm sample and $\varepsilon_\infty = 3.965$, $\omega_p = 2.93\times10^{15}$ rad/s, and $\gamma = 2.19\times10^{14}$ rad/s for the 53 nm sample].

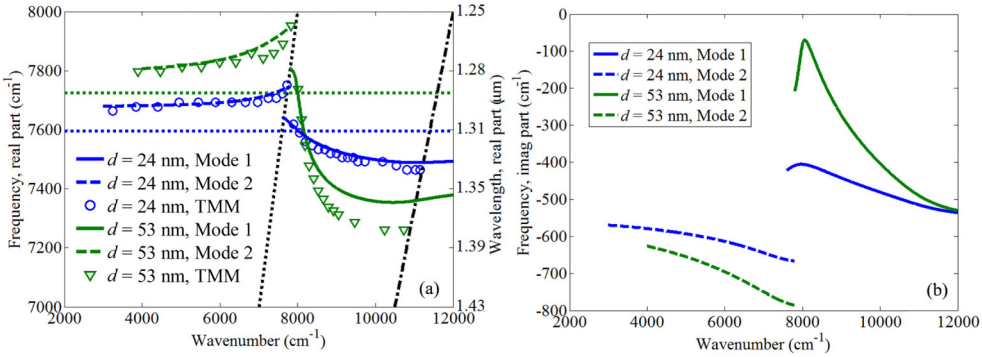

Fig. 3. (a) Real part and (b) imaginary parts of the complex-frequency/real-wavenumber dispersion diagram retrieved via eigenmode analysis (Mode 1 and Mode 2) for the two samples with thicknesses of 24 (solid and dashed blue lines) and 53 (solid and dashed green lines) nm. In panel (a), the symbols represent the TMM result similar to what shown in Fig. 2(b), now computed with the approximate Drude formula for ITO. In (a), the dotted and dash-dotted black lines refer to the light lines in free space and glass, respectively. The dotted blue and green lines indicate the ENZ crossing point for the 24 and 53 nm samples computed from the Drude permittivity models, respectively.

Application of the procedure in Eq. (1) leads to four complex eigenmodes for each real wavenumber, with each eigenmode being associated with a particular choice of signs for k_{z1} and k_{z3} [13]. In general, these four modes correspond to bound or leaky waves of the structure, with incoming or outgoing wave propagation in the bounding half spaces (i.e., media 1 and media 3). In the following we shall retain only two particular complex eigenmodes in the complex-frequency plane, as previously suggested in [15]: (1) the one decaying in both air and glass (i.e. non radiating, computed by imposing negative signs for both k_{z1} and k_{z3}) referred to as Mode 1, solid lines in Fig. 3 – *the NR-ENZ polariton mode*; and (2) the one leaky in both air and glass (i.e. radiating, computed by imposing positive signs for both k_{z1} and k_{z3}) referred to as Mode 2, dashed lines in Fig. 3 – *the R-ENZ polariton mode*. Mode 1 and Mode 2 are shown to follow the dispersion on the right and on the left of the light line, respectively. To avoid errors rising from the Drude model approximation, we recomputed in Fig. 3 the TMM result shown in Fig. 2 using the same Drude model. We find fairly good agreement in Fig. 3 between modal analysis and TMM results, suggesting that the dispersion obtained experimentally in Fig. 2(b) belongs to eigenmodes supported by the structure. In particular, we see that Mode 1 (solid blue and green lines) follows the NR-ENZ polariton dispersion on the right of the light line (blue circles and green triangles). Similarly, we see that Mode 2 (dashed blue and green lines) follows the R-ENZ dispersion on the left of the light line (blue circles and green triangles). Small differences are observed in Fig. 3, which arise from the fact that modal analysis provides modes with complex frequency, whereas in TMM results all the quantities are real, so perfect overlap would be expected in regions where the imaginary part of the complex frequency vanishes. For this reason, the TMM result does not provide the dispersion of the imaginary part of the mode, which can be computed using modal analysis as shown in Fig. 3. We further note in Fig. 3 that Mode 1 supported by the 53-nm-thick sample exhibits lower

loss than Mode 1 supported by the 24-nm-thick sample. Moreover, Mode 1 is less lossy than Mode 2.

4. Near-perfect absorption thanks to the ENZ polariton mode

We further observe that for illumination conditions close to the NR-ENZ polariton mode dispersion, the three-medium structure at hand can exhibit directional near-PA close to the ENZ frequency, as confirmed in Fig. 4. In particular, we show in Fig. 4(a) a composite view of the experimental absorption spectra [computed as 1-R above the glass-to-air critical angle, $\mathrm{asin}\left(\sqrt{\varepsilon_3/\varepsilon_1}\right)$] in the frequency band 5000–12000 cm^{-1} for the 53-nm-thick sample. Each horizontal strip in this figure represents an absorption spectrum, measured at a particular incidence angle. Figure 4(b) displays the theoretical results computed using TMM with the ITO experimental permittivity. These calculations are in good agreement with experimental results. In Fig. 4(b) we see limited absorption (up to ~50%) from normal incidence to the glass-to-air critical angle. Above the critical angle, the transmission is zero. The abrupt absorption change to ~100% right above the critical angle is due to the constructive interference of incident and reflected waves around the excitation conditions of the NR-ENZ mode. We also show on the experimental absorption map the green solid line which represents the real part of the wavenumber of the eigenmode Mode 1 in Fig. 3(a). Note that the trajectory of this eigenmode (approximate because of the Drude model for ITO permittivity) matches the absorption profile quite well, showing that the near-PA happens under illumination conditions close to the dispersion of the NR-ENZ polariton mode. Maximum absorption of 99.6% occurs at the angle of incidence of ~43.7°, which is also precisely captured by the eigenmode model. For the right sample conditions (e.g. 56.2 nm thickness and the angle of incidence of ~43.7°), perfect absorption would be achieved.

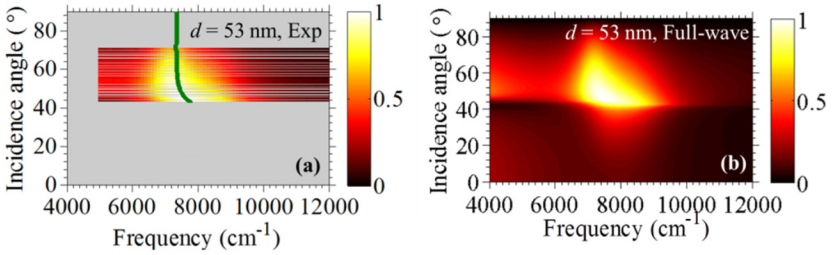

Fig. 4. Panel (a) displays the raw experimental spectra at several discrete angles and panel (b) shows results calculated from TMM simulations. In (a), the solid green curve represents the real part of the complex-frequency/real-wavenumber dispersion diagram retrieved via eigenmode analysis shown in Fig. 3(a) for Mode 1.

The near-PA in Fig. 4 manifests itself in a significant field enhancement $|E/E_0|$ within the ITO layer. We thus report in Fig. 5 the field enhancement within the ITO layer computed using full-wave simulations (COMSOL Multiphysics) versus frequency and angle of incidence for the three-medium structure for both samples under investigation. The electric field enhancement is virtually constant in the ITO film and it reaches peaks of about 3.2 and 2.5 for d = 24 and 53 nm, respectively. Favorable conditions for field enhancement processes occur in the frequency band 7000–9000 cm^{-1} and angular band 40–60 degrees. Such field enhancements may open new windows of opportunity for the enhancement of nonlinear optical processes, as recently proven experimentally for third harmonic generation [37, 38].

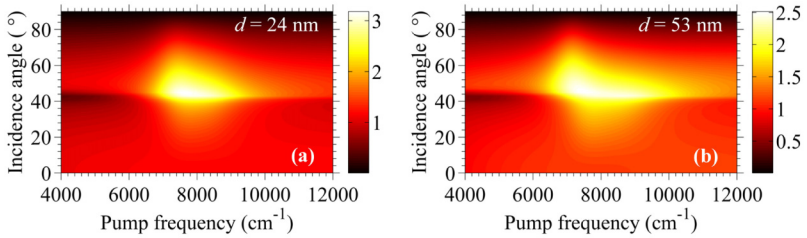

Fig. 5. Field enhancement versus frequency and angle of incidence computed using full-wave simulations at a location within the ITO layer for the three-medium structure in Fig. 1 for the two samples with thicknesses of 24 and 53 nm. Note that the electric field enhancement is virtually constant in the ITO film.

5. Conclusion

In conclusion, we have provided experimental verification of the dispersion diagrams of the R-ENZ polariton mode and, for the first time, of the NR-ENZ polariton mode supported by deep subwavelength ITO films on top of glass (no back reflector). We further confirmed that such dispersions pertain to electromagnetic eigenmodes supported by the three-medium structure. Under illumination conditions close to the dispersion of the NR-ENZ polariton mode, near-PA properties are observed. This implies the generation of a significant electric field enhancement within the ITO thin layer that can be adopted to enhance the conversion efficiency of third harmonic generation, for example. Our results further expand the list of possible material candidates that support the ENZ polariton modes, to include: diluted plasmas such as other conducting oxides; heavily doped semiconductors; reststrahlen materials just above the longitudinal optical phonon frequencies; and correlated electron materials such as vanadium dioxide.

Acknowledgments

The authors acknowledge fruitful discussions with Dr. Michael B. Sinclair, Sandia National Laboratories, and Prof. Francois Marquier, Institut d'Optique, France. Parts of this work were supported by Office of Basic Energy Science, Division of Materials Science and Engineering. This work was performed, in part, at the Center for Integrated Nanotechnologies, a U.S. Department of Energy, Office of Basic Energy Sciences user facility. Portions of this work were supported by the Laboratory Directed Research and Development program at Sandia National Laboratories. Sandia National Laboratories is a multi-program laboratory managed and operated by Sandia Corporation, a wholly owned subsidiary of Lockheed Martin Corporation, for the U.S. Department of Energy's National Nuclear Security Administration under contract DE-AC04-94AL85000. This research was performed while D.d.C. held a National Research Council Research Associateship award at the U.S. Army Aviation and Missile Research Development and Engineering Center.